Simulation of a feeder on a port-to-port mission

Ed van Daalen, Giorgio Iavicoli, Hans Cozijn, Bas de Kruif

Maritime Research Institute Netherlands
Wageningen, The Netherlands
e.f.g.van.daalen@marin.nl

Abstract—The path to autonomous shipping is paved with ambitious plans and futuristic concepts. From a realistic perspective, the transition from man-operated to machine-operated vessels depends on practical solutions for basic requirements, such as situational awareness, steerability and controllability, and flexible mission planning and execution. To develop, implement, and validate the corresponding models and the integration thereof, a generic, stable, and flexible simulation platform is needed.

This paper addresses the simulation of an autonomous feeder vessel sailing round trips between the ports of Piraeus and Mykonos. Using MARIN's simulation framework XMF, dedicated submodels are integrated into a complete model for simulation of autonomous shipping including all stages of operation, from undocking through transit to docking.

The vessel behaviour and performance during a round trip in typical weather conditions is presented and discussed.

Index Terms—short sea shipping, autonomous vessels, round trip simulation

I. Introduction

The EU MOSES project [1] aims to significantly enhance the Short Sea Shipping (SSS) component of the European container supply chain. One of the technical solutions developed in the project is an innovative container feeder vessel. The feeder design includes zero emission propulsion concepts, (semi-)autonomous operation and a robotic container handling system. The present paper presents the round trip mission (i.e. sailing from port to port and back), the various operational modes, the simulation framework and the applied submodels. In an accompanying paper [3] more details regarding the control algorithms for the autonomous operation of the container feeder are presented.

The objectives of the present study are summarised as follows:

- To investigate, implement and test autonomous operation of the container feeder, using time domain simulations, with a focus on mission execution;
- To demonstrate a complete round trip between a main port and a local port, using the implemented time domain simulation models;
- To prepare the vehicle control and vessel autonomy for future use in a pilot demonstration, where the digital model of the container feeder is replaced by a physical (scale) model.

The container feeder mission consists of a round trip between the ports of Piraeus and Mykonos. A newly developed state machine logic facilitates the split-up of the round trip into consecutive stages. A generic plugboard enables state

transitions while handing over relevant data from (for instance) a controller to its successor.

The outline of this paper is as follows: In Section II the round trip mission is defined and a detailed description of the mission execution is given. In Section III the simulation framework is introduced and detailed descriptions of the submodels are given. In Section IV a selection of simulation results is presented, with a focus on the feeder performance in terms of power usage and energy consumption. Section V contains conclusions and a brief outlook on for future research and development.

II. Mission Definition and Execution

In this section we define the mission and describe in detail how the mission is executed as a sequence of operational states, with a state machine managing the transitions.

A. Piraeus-Mykonos Round Trip

The innovative container feeder (see Figure 1) will operate in Cyclades, an island group in the Aegean Sea. The feeder will visit the islands of Kea, Syros, Tinos, Mykonos, Naxos and Paros before returning to its main port Piraeus, as illustrated in Figure 2. From the analysis of the business case it was found that in order to capture the requested demand, the feeder should perform the round trip twice a week. That led to a specific time allocation across the various segments of the round trip. In addition, a mixed pax/freight concept applied on the MOSES small Greek innovative feeder vessel was developed.
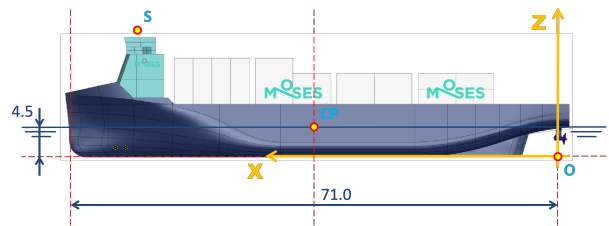

Fig. 1. Innovative container feeder.

The autonomous operation of the container feeder is investigated in calm water conditions and in an environment of combined wind and waves. For the scope of the current research the autonomous container feeder operation is greatly simplified. First off, all other traffic is excluded, both in the open sea and in the ports: distance keeping and collision
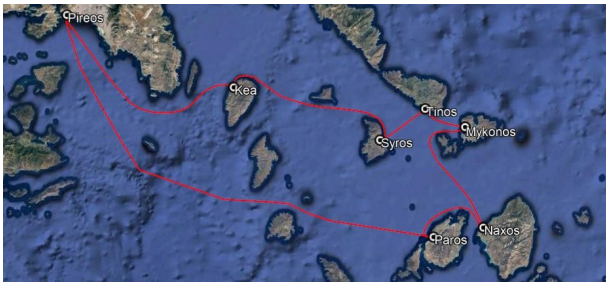
Fig. 2. The original round trip addressing Piraeus and six of the Cyclades.

avoidance strategies are not implemented. As regards the situational awareness, it is assumed that all required information (position, velocity, distance to quay) is available. Finally, a simplified mission is defined: a reduced round trip between the port of Piraeus and the port of Mykonos, as illustrated in Figure 3.
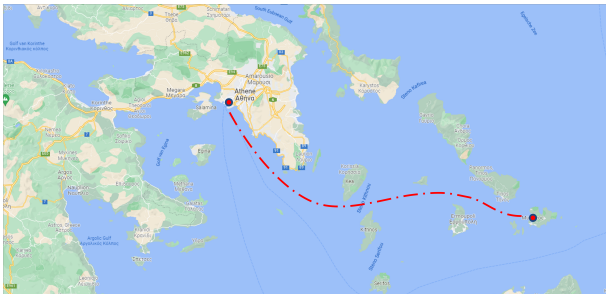

Fig. 3. The reduced round trip between Piraeus and Mykonos.

Figure 4 shows in more detail a part of the port of Piraeus and a possible feeder trajectory for arrival at the location 'Pier 3 West': the trajectory details are discussed in Section II-B. Figure 5 shows a part of the port of Mykonos and the docked feeder at the location 'Berth 7A'.

Fig. 4. Port of Piraeus. Dashed-dotted line indicates container feeder arrival at Pier 3 West.

A schematic representation of the round trip is shown in Figure 6: clearly, the distance is no longer to scale, but all relevant stages of the round trip can be distinguished, such as manoeuvring in port, docking and undocking and the transits between ports.
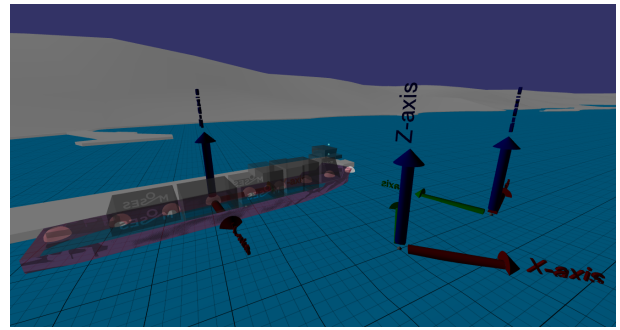

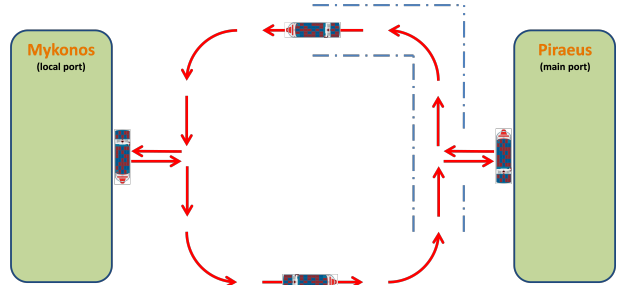Fig. 5. Port of Mykonos. Container feeder docked at Berth 7A.

Fig. 6. Schematic representation of the reduced round trip.

B. Operational Modes

The first step in modelling the autonomous operation of the container feeder is the definition of all operational modes, as shown in Figure 7. Each block represents a single operational mode of the feeder. An operational mode defines specific behaviour of the vessel, including controllers, allocators, sensors and a decision logic. At any point in time, the container feeder can be in a single operational mode only. During the round trip the vessel moves from one operational mode to another operational mode. Whether a specific transition is allowed or not depends on the current mode, the next mode and user-defined conditions, such as minimum elapsed time, matching a target position, or availability of specific subsystems. More details about the operational modes and the transitions are given in Section II-C.
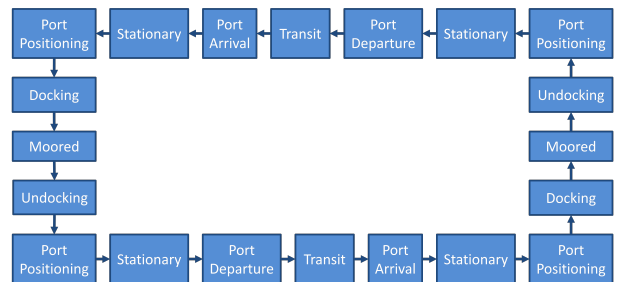

Fig. 7. The operational modes (blocks) and the transitions (arrows, in counterclockwise direction) during a full round trip.

C. Mission Execution and State Machine

For the reduced round trip we employ a simple mission execution framework, based on a state machine. Mission execution refers to the subsystem which, following a mission plan, enacts decisions depending on the feeder state (true or measured). The mission execution is implemented in Python for use in XMF simulations: it allows the user to specify a mission based on a set of operational modes, and transitions that are easily linked to properties of other nodes in the simulation. By means of such a specification, we can completely automate the decision-making process required to successfully complete the mission, as well generate a diagram for visual inspection and reference.

The mission has been decomposed into operational modes, each of which employs a specific control strategy (or 'controller') and a specific allocation strategy (or 'allocator') to perform the required task. This means that each operational mode has its own controller and allocator, as listed in Table I. Details of the controllers are given in an accompanying paper [3]. Two allocators are used: the underactuated allocator uses only main azimuthing thrusters; the fully actuated allocator uses main azimuthing thrusters and tunnel thrusters.

TABLE I
OPERATIONAL MODES WITH CONTROLLERS AND ALLOCATORS.

operational mode	controller	actuator
docked	PID-based vehicle	fully actuated
undocking	PID-based vehicle	fully actuated
transit	line-of-sight	under-actuated
approaching	cascade course	under-actuated
pre-docking	PID-based vehicle	fully actuated
docking	PID-based vehicle	fully actuated

In addition, some of the simulation parameters (such as the waypoints and the target poses for undocking and docking) depend on the location (port of Mykonos, port of Piraeus), and on the direction (arrival, departure). We decided to leave the freedom to have different number of states depending on the port, therefore the set of states will effectively be the product of the operational modes and the locations & directions. In other words: the state machine will have two copies of the same sequence of operational modes, supplemented by location & direction. This can be seen in the diagram in Figure 8, showing a UML state diagram generated automatically from the mission definition. The black dot in the upper left corner is the initial state; the grey boxes are the states (the combination of controller, allocator, and location & destination); the conditional transitions between the states are denoted by annotated arrows. The mission execution framework uses this description to make decisions. Given the current state, if all of its transition conditions are met, then the mission execution framework will shift the system to the next target state.

After the initial state we are in `mykonos_docked`. The only transition from that state has a condition that requires the feeder to remain at the dock for 180 seconds, which is checked with a stopwatch submodel. Once this condition is met, we shift to `mykonos_undocking`, which starts a trajectory out of port using the `undocking` controller. The feeder target for undocking is defined as a pose, i.e. a combination of horizontal position and orientation. After 600 seconds, we have gone far enough on DP and we shift to `piraeus_transit`, which uses an autopilot to take us to Piraeus along a predefined route. Typically, the distance between the route waypoints is 10-100 km in open sea, and it is reduced to about 0.1-1 km in port areas. When the last waypoint is reached, the port approach can start, and we shift to `piraeus_approaching`. The approach is defined as to bring the feeder towards the dock, while slowing down. When the surge velocity falls below 1 m/s, we can take advantage of the bow thrusters to improve manoeuvrability, therefore we switch to `piraeus_predocking`. The target for predocking is defined as a pose, as for the undocking. In this state, the allocator is `fullyactuated`, and the feeder can move in front of the dock. Once we reach the target pose, the controller raises the flag `predocking_finished`, and we shift to `piraeus_docking`, thus handing over control to the `docking` controller. The framework ensures that the controller hands over information to its successor in order to ensure a smooth transition, thus avoiding jumps in the control signals. The `docking` controller will then smoothly start a manoeuvre towards the dock, and will raise the flag `docking_finished` once it has successfully docked. We are now in `piraeus_docked`. Now that we have reached the same operational mode as in `mykonos_docked`, the stopwatch submodel is reset and activated. The remaining sequence of states is exactly like the one described above, but now from Piraeus to Mykonos.
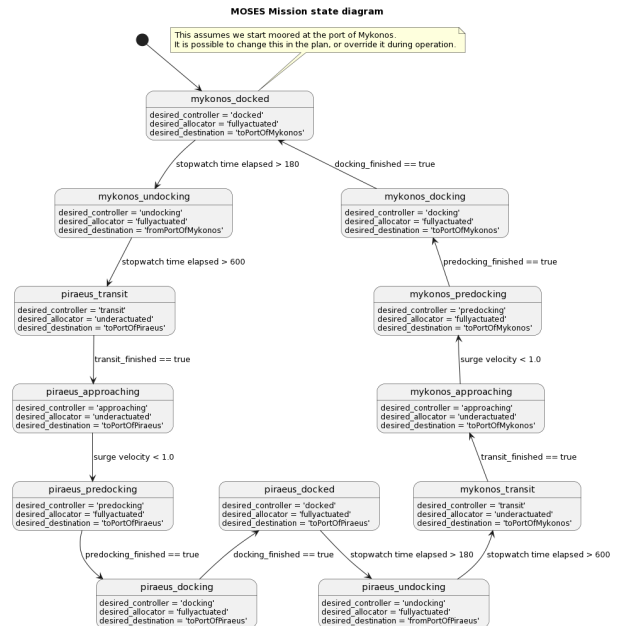

Fig. 8. Reduced round trip mission state diagram.

III. Modelling and Simulation

In this section we discuss the various submodels and their integration on the simulation framework. Most of these submodels are related to the hydrodynamic interaction of the feeder with its environment, such as the waves and the quay fenders.

A. XMF Simulation Framework

The eXtensible Modelling Framework (XMF) is a C++ software toolkit on which all MARIN's time domain simulation software developments are based. The XMF core libraries focus on reusability, extensibility, object interoperability, I/O and Newtonian dynamics. The XMF system reads the models from the input files, loads the related dynamic content libraries and starts executing a fast-time or scaled wall-clock time simulation.

The time-domain simulation model of the autonomous container feeder was built using XMF, with additional scripting and programming components (using LUA and Python). The overall structure of the simulation model is shown in Figure 9.
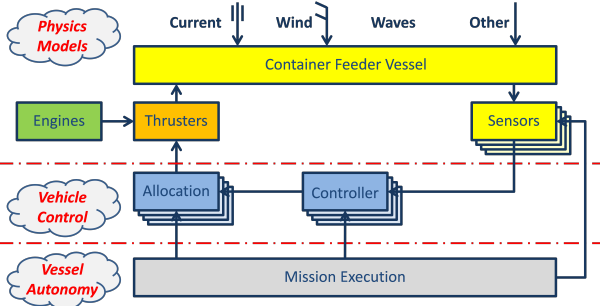

Fig. 9. Time domain simulation model structure.

The following main model groups can be distinguished:

- The 'Physics Models' group contains the models describing the vessel motions caused by external forces acting on the vessel (e.g. waves). Models for sensors and actuators are also included: some of these models are user-scripted.
- The 'Vehicle Control' group contains the models describing the vehicle control systems, such as the dynamic positioning system (for station keeping) and the autopilot (for course keeping during transit). The controller models are grouped in a so-called 'controller set' and the allocation models are grouped in a so-called 'allocator set'.
- The 'Vessel Autonomy' group contains mission execution algorithms, implemented in Python. Mission execution controls the operational state of the vessel, as well as the state transitions. Furthermore, it activates and deactivates controllers, allocators, sensors and actuators.

The XMF time domain simulation model was configured using mostly existing simulation nodes, with some additional scripting. No new functionality was implemented during the MOSES project. Nevertheless, several new aspects were considered in the present simulation study, often related to new combinations of existing models. The simulation model of the feeder includes manoeuvring forces, wave forces, wind forces, thrusters, sensors and fenders.

B. Equations of Motion

The vessel equations of motion are based on rigid body dynamics and potential flow theory. They describe the time-varying motion response (in six degrees of freedom: three translations and three rotations) of a floating structure subjected to waves and wind. The equations of motion are written as

$$\sum_{j=1}^{6} \left[\left(M_{ij} + A_{ij}^\infty \right) \ddot{x}_j \left(t \right) + \int_{-\infty}^{t} R_{ij} \left(t - \tau \right) \dot{x}_j \left(\tau \right) \mathrm{d}\tau \right. \\ \left. + C_{ij} x_j \left(t \right) \right] = F_j \left(t \right)$$

where

- the indices i, j denote the modes: 1=surge, 2=sway, 3=heave, 4=roll, 5=pitch, 6=yaw;
- x is the motion response;
- F is the total external force;
- M is the vessel inertia matrix: mass and moments of inertia;
- A^∞ is the 'added mass at infinite frequency' matrix;
- R is the matrix of retardation functions;
- C is the matrix of hydrostatic restoring forces.

The retardation functions and the added mass at infinite frequency matrix are determined using the results of linear radiation(-diffraction) calculations.

XMF time-domain simulations often concern either a ship sailing at a constant speed (e.g. seakeeping or manoeuvring calculations), or a floating object at a stationary location (e.g. a floating wind turbine, or a ship with a DP system). These simulation studies concern (quasi-)stationary conditions for a limited amount of time (e.g. 3hr simulations for a moored ship in wind waves and current). In the MOSES project, however, the Piraeus-Mykons round trip simulations have a long duration and include instationary conditions. Therefore, zero speed models and forward speed models had to be combined in a consistent way. Also, potential double-countings were identified and resolved, for instance in the calculation of manoeuvring forces and seakeeping forces in the low-frequency range.

C. Gravity and Hydrostatic Forces

The feeder is subject to the Earth's gravity field, with the gravity force acting vertically downwards. The buoyancy is calculated with a linear hydrostatics model. The vessel has a waterline area, which creates a restoring force in the heave mode and restoring moments in the roll and pitch modes. The motions are assumed to be small: therefore the hydrostatics can be linearized about the vessel equilibrium position and orientation. The main particulars and stability data are listed in Table II.

description	value	
length between perpendiculars	71.000	m
length on waterline	72.533	m
beam	13.000	m
draft	4.500	m
displacement volume	2899	m^3
block coefficient	0.718	-
waterline area	812.824	m^2
longitudinal center of gravity from APP	34.406	m
vertical center of gravity from keel	5.593	m
vertical center of buoyancy from keel	2.487	m
transverse metacentric height	0.429	m
longitudinal metacentric height	92.328	m
roll radius of gyration	4.550	m
pitch radius of gyration	17.750	m
yaw radius of gyration	17.750	m

D. Manoeuvring Forces

A theoretical-empirical manoeuvring model with CFD-based coefficients accounts for nonlinear hull forces due to steady to low-frequent motions in the horizontal modes, i.e. surge, sway and yaw. A ship moving through the water experiences hydrodynamic forces, which depend on the surge, sway and yaw velocities. These forces include the calm water resistance and the manoeuvring forces. In the time domain simulation model these forces are represented by a coefficient model. The manoeuvring coefficients are determined using MARIN's CFD software ReFRESCO [4]. The calculations are done for a single forward speed and various combinations of drift angle and rate of turn. An example of the output is shown in Figure 10, showing the hull pressure coefficient.
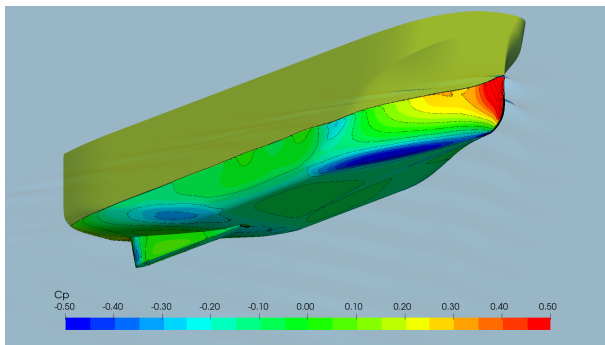

Fig. 10. Hull pressure coefficient C_p. Result obtained with MARIN's CFD software ReFRESCO [4].

Next, the manoeuvring coefficient model is derived through the following steps:

- Fitting of polynomial functions through the discrete points from the CFD calculations. The coefficients included in the curve fitting are selected based on knowledge of ship hydrodynamics. Furthermore, the number of coefficients is limited to avoid overfitting. An example is shown in Figure 11.

- The CFD calculations are done for a single forward speed. The speed dependent longitudinal force was compared with the resistance curve obtained with MARIN's DESP program [5]. To achieve a better correspondence at higher forward velocities, an extra coefficient was introduced in the manoeuvring model. The resulting resistance curve is shown in Figure 12.
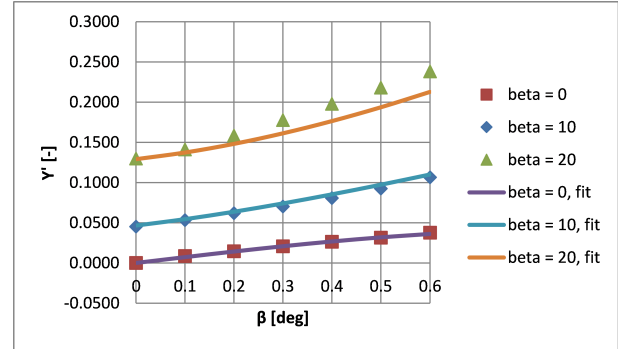

Fig. 11. Manoeuvring model coefficient fit for the dimensionless sway force as function of the drift angle.
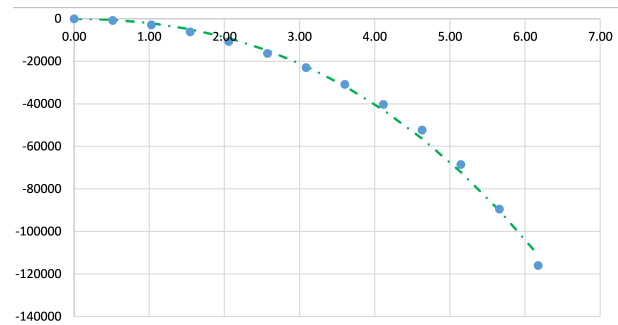

Fig. 12. Resistance curve with additional coefficient. Result from CFD software ReFRESCO [4] and DESP [5]. Horizontal axis: speed [m/s]. Vertical axis: resistance [N].

E. Wave Radiation Forces

As a result of its own motions the vessel will experience hydrodynamic reaction forces from the surrounding water. The hydrodynamic reaction forces are represented by added mass coefficients (corresponding to the in-phase component) and damping coefficients (corresponding to the out-of-phase component). The added mass and damping coefficients are pre-calculated with the linear frequency domain codes DIFFRAC [6] (for zero speed) and SEACAL (for forward speed: 3.9kn, 7.8kn, 11.7kn) and stored in databases. An example of the output is presented in Figure 13. At the start of the simulation, the added mass and damping coefficients are read and then transformed to their time-domain equivalents, i.e. the added mass at infinity coefficients and the retardation functions.

F. Extra Roll Damping Forces

In addition to the roll damping due to motion-induced (radiated) waves, there is roll damping from other sources, e.g.
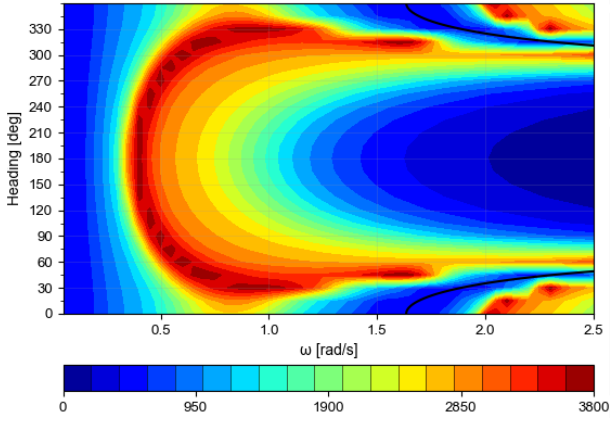
Fig. 13. Heave damping coefficient at 12kn speed. Result obtained with linear frequency domain seakeeping program SEACAL.

hull friction forces and bilge keel drag and lift forces. These effects are not included in the results from linear frequency domain calculations. This extra roll damping is represented by a linear and a quadratic roll damping coefficient:

$$F_{4,\text{extra}}(t) = - \left[B_{44,\text{extra}}^{(1)} + B_{44,\text{extra}}^{(2)} |p(t)| \right] p(t)$$

where p dentotes the roll (angular) velocity. The linear and quadratic coefficients are calculated from roll decay model tests with similar vessels. The roll damping coefficients are assumed to be independent of speed, which is a conservative approach: the roll damping may increase with speed due to lift forces on the hull and the bilge keels.

G. Wave Excitation Forces

The software codes DIFFRAC and SEACAL - both based on three-dimensional linear radiation-diffraction theory - provide the frequency domain transfer functions of the first and second order wave excitation forces. The wave excitation forces are calculated for zero speed up design speed and for deep water ('open sea') and shallow water ('port areas'). Due to incoming waves the vessel will experience first order wave excitation forces, represented by linear transfer functions (amplitude and phase). These transfer functions are pre-calculated for various speeds (0kn, 3.9kn, 7.8kn, 11.7kn) and headings (from 0deg to 360deg with a 15deg step) and stored in databases. At the start of the simulation the transfer functions are read; during the simulation (at each time step) they are used to calculate the wave excitation forces.

Besides the first order wave excitation forces the vessel will also experience second order wave excitation forces. The second order wave excitation forces are the mean and low frequency wave contributions, which are associated to difference frequencies of pairs of incoming wave components. The second order wave excitation forces are represented by Quadratic Transfer Functions (QTFs). They are stored as in-phase and out-of-phase components. These transfer functions were calculated in the same frequency domain linear diffraction calculations as the wave radiation forces and the first order
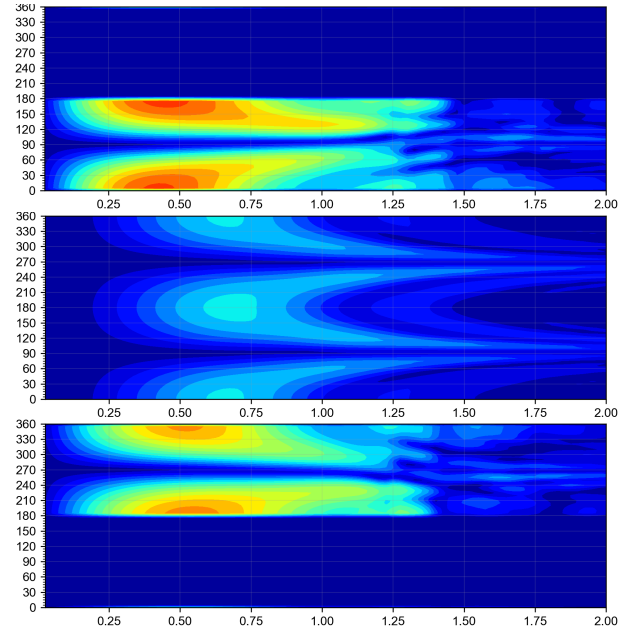

Fig. 14. First order wave excitation surge force. Top: port of Mykonos. Center: open sea. Bottom: port of Piraeus. Horizontal axis: wave frequency [rad/s]. Vertical axis: wave direction [deg].

wave excitation forces. Again, the calculations were performed for all motion components and for all wave directions. The calculation results were stored in the same databases. During the time domain simulations, the frequency domain QTFs are read from the different databases and used to create time traces of the second order wave excitation forces.
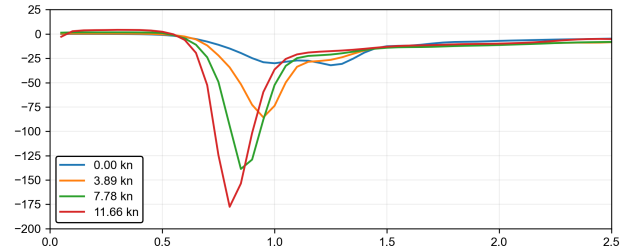

Fig. 15. Surge drift force. Horizontal axis: wave frequency [rad/s]. Vertical axis: surge drift force [kN/m²].

Based on the vessel position ("in open water", "in port of Mykonos", or "in port of Piraeus") and speed an interpolation may be made between the wave loads calculated based on the different databases. The procedure is as follows:

- At both ports two reference radii are defined, R_{quay} and R_{port}. During the simulation, the distance d between the ship and the intended mooring location at the berth is calculated. The reference radii define which combination of wave force databases is used, depending on the vessel position.
- The wave forces are calculated using the diffraction database associated with the vessel moored at the quay side when $d < R_{\text{quay}}$. The wave forces are calculated

using the diffraction database associated with open water when $d > R_{port}$. In between ($R_{quay} < d < R_{port}$) an interpolation is made between both databases, using a cosine taper function, as shown in Figure 17.
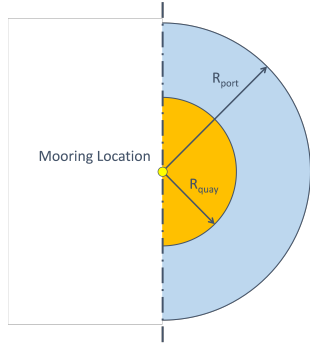

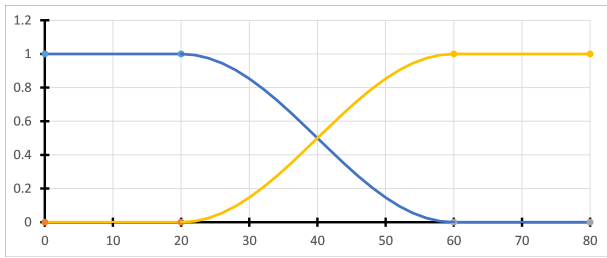Fig. 16. Definition of quay reference radius and port reference radius.

Fig. 17. Example of interpolation factor: $R_{quay} = 20$m, $R_{port} = 60$m.

Figure 18 shows the wave scatter diagram for the port of Piraeus. Based on this diagram, and similar diagrams for the port of Mykonos and for the open sea, the probability of exceedance of the significant wave height can be calculated. This enables the selection of representative wave parameters.
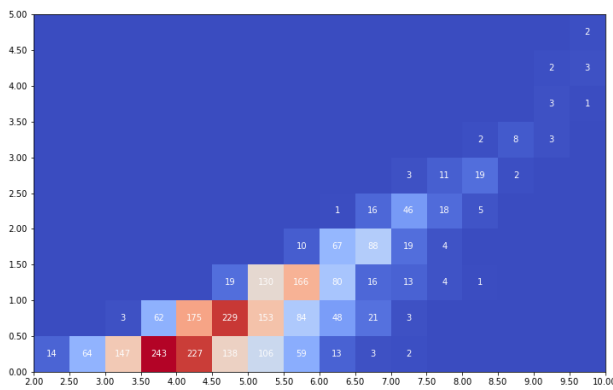

Fig. 18. Port of Piraeus - Wave scatter diagram. Horizontal axis: peak wave period [s]. Vertical axis: significant wave height [m]. The numbers in the squares indicate the probability of occurrence (sum = 1000).

H. Wind Forces

In a wind field the vessel will be subjected to wind forces. The magnitude and direction of the wind forces will depend on the relative (apparent) wind speed and direction, based on the absolute wind speed & direction and the vessel speed & heading. The wind forces are proportional to the relative wind speed squared. The calculation of the wind forces is based on vessel-specific (dimensionless) wind load coefficients. The feeder's wind load coefficients are determined with MARIN's CFD code ReFRESCO [4]. Figure 19 shows the wind load coefficients for the surge & sway motions and the roll & yaw moments.
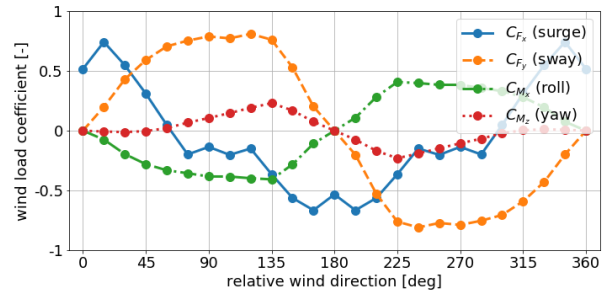

Fig. 19. Dimensionless wind load coefficients for surge & sway forces and roll & yaw moments as a function of relative wind direction.

Figure 20 shows the wind scatter diagram for the port of Piraeus. Based on this diagram, and similar diagrams for the port of Mykonos and for the open sea, the probability of exceedance of the wind speed can be calculated. This enables the selection of representative wind parameters.
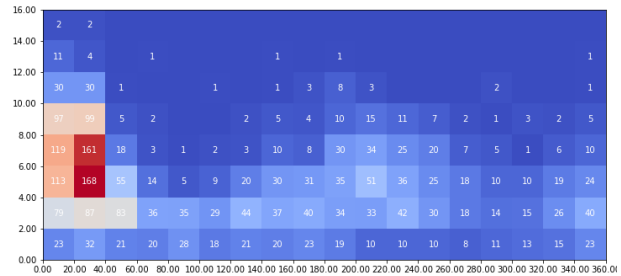

Fig. 20. Port of Piraeus - Wind scatter diagram. Horizontal axis: wind direction [deg]. Vertical axis: wind speed [m/s]. The numbers in the squares indicate the probability of occurrence (sum = 1000).

I. Current Forces

Sea currents are not considered in the present simulations. Inside the ports the current velocities are assumed to be negligible. At open sea, the current velocities are assumed to be much smaller than the vessel speed.

J. Azimuthing Thrusters and Tunnel Thrusters

The feeder vessel is equipped with two azimuthing thrusters and two bow tunnel thrusters. The modelled thruster forces include the propeller thrust and torque. These are calculated using four-quadrant propeller diagrams, available from a propeller database. For the azimuthing thrusters rpm (rate of turn) and azimuth angle set-points can be specified. The azimuth response is limited by a maximum rotation speed, while the

propeller rpm response is calculated by a dynamic engine model. For the bow tunnel thrusters an rpm set-point can be specified. The propeller rpm response is calculated by a dynamic engine model. The thruster properties are presented in Table III.

description	value	
diameter (azimuthing)	1.5	m
azimuthing thruster maximum power	49	MW
azimuthing thruster maximum rpm	644	min^{-1}
azimuthing thruster rudder speed	18	deg/s
tunnel thruster diameter	1.0	m
tunnel thruster maximum power	200	kW
tunnel thruster maximum rpm	786	min^{-1}

The thrusters are used to control the vessel in the horizontal plane. The allocation algorithm distributes the required horizontal forces and the yaw moment over the available thrusters. Bow tunnel thrusters become less effective with increasing forward speed. The allocation strategy accounts for this, by using the tunnel thrusters only at speeds below 1 m/s. Above this threshold only the main azimuthing thrusters are used. Summarizing: At low speeds all thrusters are used and the vessel is fully actuated. At speeds above 1 m/s only the main azimuthing thrusters is used and the vessel is under-actuated.

K. Sensors

To obtain specific quantities, such as position and velocity, at reference points, sensors are used. These sensors are used for logging, for motion control purposes, or for evaluating motion-based criteria. To enable camera-guided docking, a 'pose sensor' model was developed, which calculates the vessel position and orientation in the horizontal plane with respect to a reference frame attached to the quay. Table IV lists the sensors with details on the type & purpose, location and coordinates.

TABLE IV
SENSOR PARAMETERS: COORDINATES ARE WITH RESPECT TO AFT PERPENDICULAR, CENTER, KEEL. SB = STARBOARD SIDE, PS = PORT SIDE. COORDINATES ARE GIVEN IN METERS.

type, purpose	location	coordinates
motions, logging	CoG	(34.406, 0.000, 5.639)
motions, navigation	mast	62.500, 0.000, 18.000)
wind, navigation	mast	(62.500, 0.000, 18.000)
motions, criteria	bridge	(62.500, 0.000, 15.000)
motions, control	control point	(35.500, 0.000, 4.500)
motions, logging	aft SB	(9.571, -2.264, 15.900)
motions, logging	aft PS	(9.571, 2.264, 15.900)
motions, logging	fore SB	(53.818, -4.324, 15.120)
motions, logging	fore PS	(53.818, 4.324, 15.120)

L. Fenders

The interaction between the vessel and a fender is based on the geometrical intersection of a 'fendermesh' (a set of polygons attached to the vessel) and a sphere representing the fender geometry. The fender model calculates the contact properties and associated reaction forces: the spring force is calculated from the fender compression and the damping force is calculated from the relative normal velocity at the contact point.

The quay in the port of Piraeus is equipped with 11 fenders equally spaced (10m apart). The quay in the port of Mykonos is equipped with 9 fenders equally spaced (10m apart). Table V lists the fender parameters. Figure 21 shows the fender compression force as a function of the compression. Clearly, this is a non-linear relation.

TABLE V
FENDER PARAMETERS.

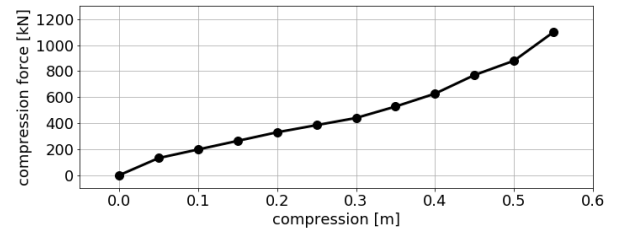| description	value	
diameter	2.0	m
horizontal friction coefficient	0.125	-
vertical friction coefficient	0.125	-

Fig. 21. Fender compression force as a function of compression.

IV. RESULTS

The results shown below apply to a full round trip in wind and wave conditions corresponding to 50% probability of exceedance. The waypoints are chosen such that the route is in bweeen the Cyclades. The westbound and eastbound routes are about two miles apart. The round trip takes about 26 hours.

Figure 22 shows the vessel's global position with zoomed in views of the manoeuvres in both ports.
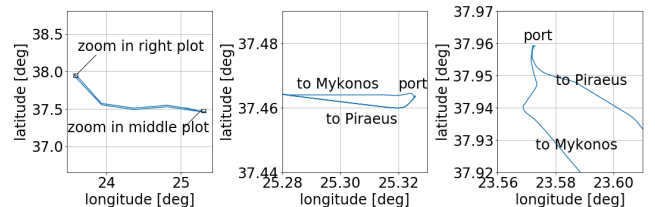

Fig. 22. Global position in latitude-longitude. Left: round trip. Center: port of Mykonos arrival & departure. Right: port of Piraeus arrival & departure.

Figure 23 shows the feeder's speed over ground. During the transit stages the 10kn design speed is maintained well. In the approaching, pre-docking, docking and undocking stages the speed is reduced significantly for better manoeuvring and dynamic positioning.
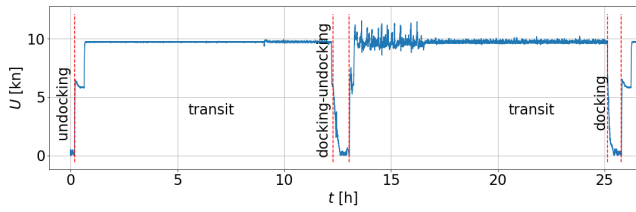
Fig. 23. Speed over ground. Vertical dashed lines indicate transitions from and to transient stage.
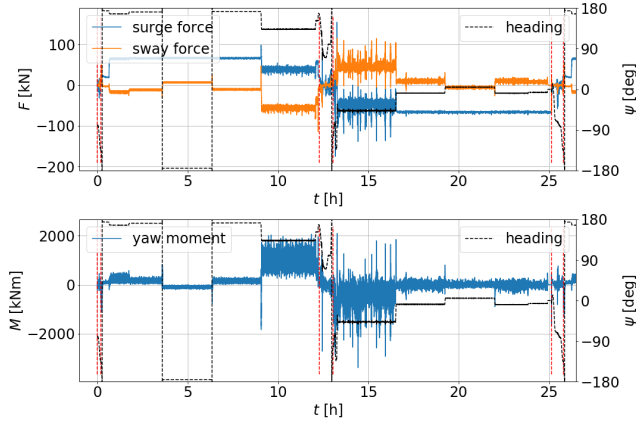

Fig. 24. Manoeuvring forces. Top: surge & sway forces. Bottom: yaw moment. Vertical dashed lines indicate stage transitions, see Figure 23. (Heading plotted against right vertical axis for easier interpretation.)

Figure 24 shows the surge, sway and yaw components of the manoeuvring forces, which are strongly correlated with the heading of the feeder.

The extra roll damping coefficients are set at $B_{44,\text{extra}}^{(1)} = 3 \times 10^6$ (linear) and $B_{44,\text{extra}}^{(2)} = 0$ (quadratic). Figure 25 shows the roll angle & velocity and the resulting roll moment.
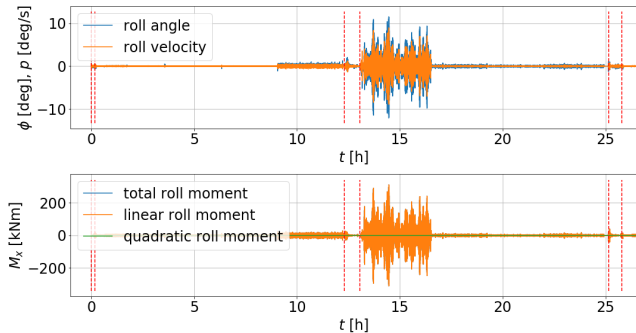

Fig. 25. Extra roll damping. Top: roll angle and roll velocity. Bottom: linear and quadratic roll moment. Vertical dashed lines indicate stage transitions, see Figure 23.

The wind speed and direction are set at constant values of 6.7m/s and 0deg, i.e. from the East. Figure 26 shows the wind forces and moments with a clear distinction between westbound and eastbound transient stages.

A JONSWAP wave spectrum with a significant wave height of 0.5m and a peak wave period of 3.75s is selected. There are no waves due to swell. Figure 27 shows the wave excitation
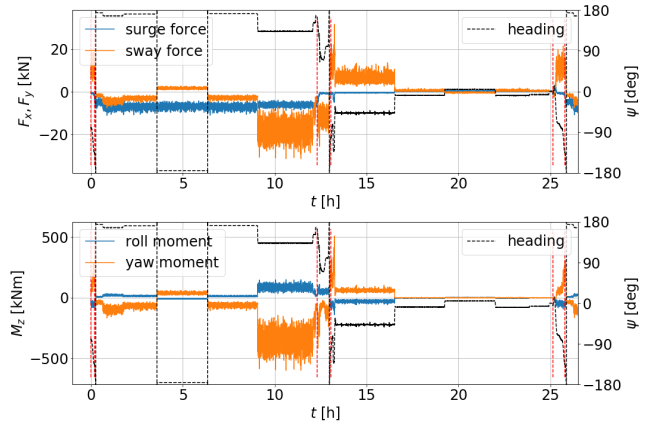

Fig. 26. Wind forces. Top: surge & sway forces. Bottom: roll & yaw moments. Vertical dashed lines indicate stage transitions, see Figure 23. (Heading plotted against right vertical axis for easier interpretation.)

forces. As expected, there is a strong correlation between the heading and the first order roll moment. Also, there is a strong correlation between the heading and the second order surge force.
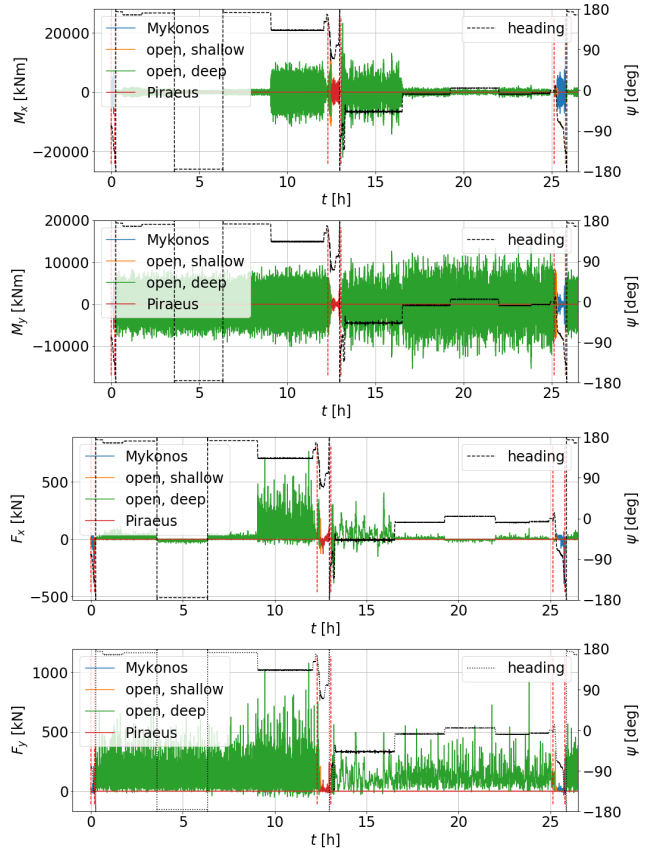

Fig. 27. Wave excitation forces. From top to bottom: first order roll moment, first order pitch moment, second order surge force, second order sway force. Vertical dashed lines indicate stage transitions, see Figure 23. (Heading plotted against right vertical axis for easier interpretation.)

Figure 28 shows the fender forces in the port of Piraeus during the docking and docked stages. Clearly, the compression effect is dominant over the friction effect. Note that the

compression force is always non-negative, whereas the friction force can take both positive and negative values.
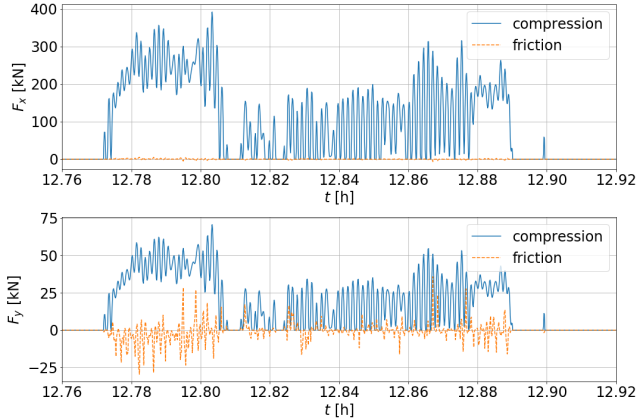

Fig. 28. Fender compression and friction forces during docking and docked stages in the port of Piraeus. Top: surge force. Bottom: sway force.

Figure 29 shows the power and energy consumption of the azimuthing thrusters, the tunnel thrusters and all thrusters. The total energy consumption in a round trip is 9.43 MWh. The energy consumption in the transit stages is 9.20 MWh, which is 97.5% of the total. The azimuthing thrusters consume 99.4%, leaving 0.6% for the tunnel thrusters which are only active in the relatively short pre-docking, (un)docking and docked stages.
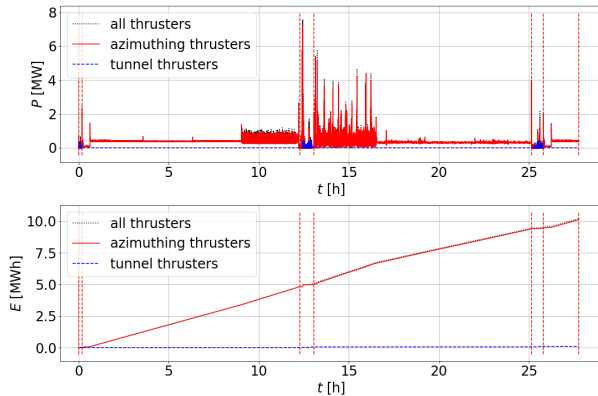

Fig. 29. Performance evaluation. Top: power usage. Bottom: energy consumption. Vertical dashed lines indicate stage transitions, see Figure 23.

V. CONCLUSIONS

In this paper we described the motivation, approach and results of computer simulations of an autonomous feeder on a round trip between the ports of Pireaus and Mykonos. The simulation model is based on a divide-and-conquer approach: the round trip is split up into successive stages and for each stage dedicated motion control submodels are used. A newly developed state machine keeps track of the vessel's progress and makes decisions to deactivate and activate controllers, allocators and sensors, based on user-specified conditions. To ensure smooth stage transitions data (such as position, velocity) can be transferred from a submodel to its successor.

MARIN's eXtensible Modelling Framework (XMF) was used to build a time domain simulation model of the autonomous feeder. Existing submodels were used to create a digital environment (ports, waves, wind) and a digital model of the feeder, including thrusters and sensors. The underlying equations of motion include gravity and hydrostatic forces, manoeuvring forces, extra roll damping forces, first and second order wave excitation forces, wind forces and forces due to mechanical interaction with quay fenders. The calculation of these force components was done on the basis of experience built up over many years, using state-of-the-art computational tools such as MARIN's CFD software ReFRESCO.

This approach enables the simulation of complex missions and the design of configurable, re-usable components before they are tested with hardware. The next step is to put the innovative feeder concept to the test in our experimental facilities in September 2023.

REFERENCES

[1] MOSES: Automated Vessels and Supply Chain Optimisation for Sustainable Short Sea Shipping, https://moses-h2020.eu/, March 20, 2023.
[2] A. Abbing, "XMF leads to development of a multi-purpose simulation platform," MARIN Report 116, December 2015.
[3] B.J. de Kruif, E.F.G. van Daalen, H. Cozijn, G. Iavicoli, "Control of all steps in a quay-to-quay mission for a feeder vessel," OCEANS 2023, Limerick (submitted abstract).
[4] https://www.marin.nl/en/facilities-and-tools/software/refresco, April 20, 2023.
[5] https://www.marin.nl/en/about/facilities-and-tools/software#motion, April 20, 2023.
[6] https://www.marin.nl/en/facilities-and-tools/software/diffrac, April 20, 2023.